Master of Science Thesis in Control and Information Systems
Department of Electrical Engineering, Linköping University, 2021

Airborne Angle-Only Geolocalization

Tove Kallin

LINKÖPING UNIVERSITY

Master of Science Thesis in Control and Information Systems

Airborne Angle-Only Geolocalization

Tove Kallin

LiTH-ISY-EX--21/5385--SE

Supervisor: **Robin Forsling**
ISY, Linköping university
Fredrik Andersson
Saab AB

Examiner: **Fredrik Gustafsson**
ISY, Linköping university

Division of Automatic Control
Department of Electrical Engineering
Linköping University
SE-581 83 Linköping, Sweden

If it's time to go, remember what you're leaving. Remember the best.

Abstract

Airborne angle-only geolocalization is the localization of objects on ground level from airborne vehicles (AV) using bearing measurements, namely azimuth and elevation. This thesis aims to introduce elevation data of the terrain to the airborne angle-only geolocalization problem and to demonstrate that it could be applicable for localization of jammers. Jammers are often used for deliberate interference with malicious intent which could interfere with the positioning system of a vehicle. It is important to locate the jammers to either avoid them or to remove them.

Three localization methods, i.e the nonlinear least squares (NLS), the extended Kalman filter (EKF) and the unscented Kalman filter (UKF), are implemented and tested on simulated data. The methods are also compared to the theoretical lower bound, the Cramér-Rao Lower Bound (CRLB), to see if there is an efficient estimator. The simulated data are different scenarios where the number of AVs, the relative flight path of the AVs and the knowledge of the terrain can differ. Using the knowledge of the terrain elevation, the methods give more consistent localization than without it. Without elevation data, the localization relies on good geometry of the problem, i.e. the relative flight path of the AVs, while the geometry is not as critical when elevation data is available. However, the elevation data does not always improve the localization for certain geometries.

There is no method that is clearly better than the others when elevation data is used. The methods' performances are very similar and they all converge to the CRLB but that could also be an advantage. This makes the usage of elevation data not restricted to a certain method and it leaves more up to the implementer which method they prefer.

Acknowledgments

This thesis marks the end of my education and an end of a journey as well as a beginning of a new one. Throughout my education I have met wonderful friends and a loving partner who have supported me and given me many fun memories that I will look back to all my life. I want to thank my family for having an unwavering faith that I would overcome any obstacle. I would also want to thank my supervisors, Fredrik Andersson and Robin Forsling, for great help on my thesis. I have always been able to talk to you when I have been lost or confused which made this thesis possible. It was also very motivating that Fredrik Gustafsson, the examiner, took an active roll in the thesis and held interest in the project. In the end, I am very proud of this achievement and I am thankful for every person I have met. I would not have been able to do half of the things I have done, if I would not have met all of you.

Linköping, June 2021
Tove Kallin

Contents

Notation

Some terminology

Word	Meaning
Target	The targets in this thesis refer to objects that generate or emit signals. It could, for example, be an object that emits a radio frequency, such as a jammer, that can be used as an interference for GNSS.
Receiver	The receivers are the devices that receive and interpret the signals as well as estimate the direction to the targets. Their position and orientation are known. In this thesis they are AVs of some kind.

Abbreviations

Abbreviation	Meaning
2D	Two dimensions
3D	Three dimensions
AV	Airborne Vehicle/Aerial Vehicle
CRLB	Cramér–Rao Lower Bound
DOA	Direction Of Arrival
EKF	Extended Kalman Filter
FIM	The Fisher Information Matrix
KF	Kalman Filter
GNSS	Global Navigation Satellite System
NLS	Nonlinear Least Squares
NWLS	Nonlinear Weighted Least Squares
RMSE	Root Mean Square Error
SAR	Search And Rescue
UAV	Unmanned Aerial Vehicle
UKF	Unscented Kalman Filter
UT	Unscented Transform
WGN	White Gaussian Noise

Mathematical notations

Notation	Meaning
$\hat{x}$	Estimated value of x.
μ_x	Mean value of x.
$\mathcal{N}(x; \mu, \sigma^2)$	The normal distribution associated with x has mean μ and standard deviation σ.
$\mathbb{R}$	Real numbers.
$\mathbb{R}^+$	Positive real numbers.
$\frac{\partial}{\partial x}$	Partial derivative with aspect to x.
$\mathrm{tr(A)}$	The trace of a matrix A.
$\mathbf{E}[x]$	The expected value of x.
$\mathrm{cov}(x)$	The covariance of x.
$\|x\|_2$	The Euclidean norm (two-norm) of x.

Variables

Variable	Meaning
α	Azimuth angle
ϵ	Elevation angle
ϕ	Roll angle
θ	Pitch angle
ψ	Yaw angle
e	Measurement error
q	Orientation of the receiver
$\mathbf{R}(q)$	Rotation matrix
w	Process noise
x	Position of target in the static global coordinate system
x_r	Position of target relative to the receiver
y	Position of the receiver
z	Measurements

1

Introduction

Jammers are devices that intentionally interfere with wireless communication, such as GNSS[1], often with malicious intent. Interference can lead to, for example, inaccurate positioning, which makes it important to locate the jammers to either avoid them or to remove them. There could also be unintentional interference, which could result in a similar problem, and the same type of solution could be applied.

This thesis focuses on locating jammers from airborne vehicles (AV) which can measure the bearing to a static ground level jammer. By only using the measured directions to the jammer, this becomes an angle-only localization problem and this thesis also introduces the usage of elevation data of the terrain to see if the geolocalization can be improved.

The methods presented are not only applicable to locate jammers, they are presented in such way that any kind of airborne angle-only geolocalization problem could use the same solutions. One such problem where these solutions could be applicable is the search and rescue (SAR) problem, where it is usual to use airborne vehicles (AV) to locate people. Although, it is not too common to use bearing measurements in SAR yet, some investigation has been made to see how SAR can be improved by it (see for example Fei et al. (2020)). To evaluate the methods, a simulation system is built and the results are compared to a theoretical lower bound using Cramér-Rao Lower Bound (CRLB).

[1] Global Navigation Satellite System.

1.1 Background

This report is a part of the graduation work for a M.Sc. in applied physics and electrical engineering with specialization in control and information systems at Linköping University. The report is made possible with the cooperation of Saab Aeronautics that expressed interest in investigating the localization of jammers using AVs.

For clarity, the targets refer to the devices which we want to locate and they emit a signal. The receivers are the airborne devices, either unmanned aerial vehicle (UAV), helicopters or airplanes, that receive the targets' signal. The signal could be any kind of signal that the receivers can read, such as a radio frequency (RF) or a Wi-Fi connection request.

1.2 Problem Formulation

The main aim with this thesis is to locate a stationary ground target using airborne receiver(s) with bearing measurements to the target. The bearing is measured by the azimuth angle and elevation angle, illustrated in Figure 1.1. The receivers fly over a preplanned path towards their primary goal. A primary goal might be to arrive at a certain location or finish a mission. During this flight, the receivers pick-up a jamming signal. Luckily, the receivers are equipped with, for example, antenna arrays or other equipment which can measure the bearing towards the jammer. Therefore, the receivers secondary goal is now to locate the target, which it will hopefully do at the same time as its primary mission. The localization is made in real-time, where the estimation of the jammer's position should become better for each new sample update. Using this information, the receivers could change path to avoid the jamming or save its position for later use.

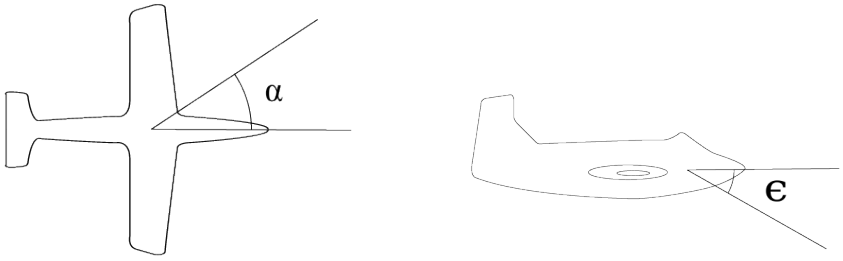

(a) *Azimuth angle, α.* ***(b)*** *Elevation angle, ϵ.*

Figure 1.1: *The directions available for the AV.*

There are many ways this angle-only geolocalization problem can be solved, but is there a general method that works for different scenarios and if so how good are those methods? Furthermore, if there is available elevation data of the terrain, could the estimations become better? This thesis aims to answer these questions. The specific assumptions for the localization are summarized below.

Goal: Locate a target on the ground
Assumptions:

1. The receivers are airborne.
2. The position and orientation of the receivers are known.
3. Target is assumed to be on ground level and is stationary.
4. The receivers can move in 3D.
5. Estimation of the position of the target should be made in real-time with updates for every new sample.
6. A target can be modelled as a point.
7. A target generates at most a single measurement per time step.
8. The receivers fly over a preplanned path.
9. Elevation data will be available for some scenarios.

1.3 Direction of Arrival

The direction of arrival[2] (DOA) consists of two measurements, the azimuth angle and the elevation angle. These two signals are measured with some additive error included. Let their true angles be described by α[3] and ϵ[4], then the measured DOA can be formulated as

$$z = \begin{bmatrix} \alpha \\ \epsilon \end{bmatrix} + \text{disturbance} \tag{1.1}$$

As the angle measurements have some disturbance, the possible position can be within a certain range. An illustration of this range is shown in Figure 1.2.

[2] Also known as bearing.
[3] Azimuth.
[4] Elevation.

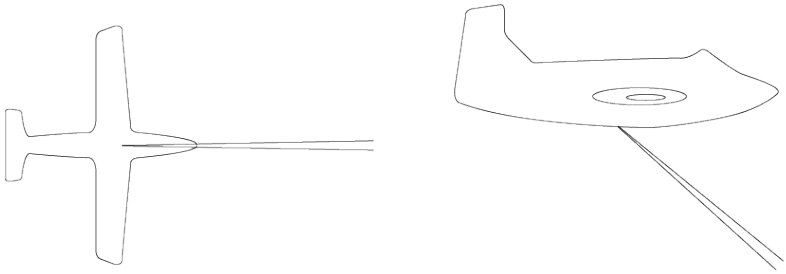

(a) *Possible range of the azimuth angle.*

(b) *Possible range of the elevation angle.*

Figure 1.2: *The possible position of the target from different perspectives.*

With two receivers, it is now possible to estimate the position of the target. To introduce this visually, it is easier to focus on the 2D version of the problem first. Figure 1.3 is taken in one snapshot. The two receivers measure the bearing with some uncertainty. Their measurements can be seen as "beams" that cross each other where the target is most likely located.

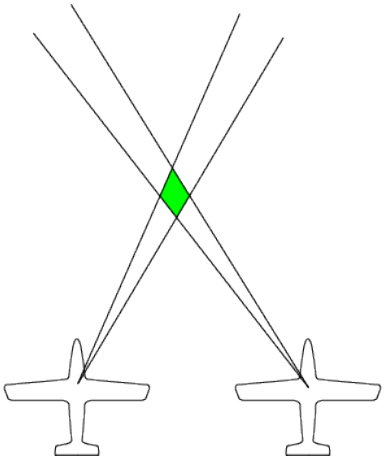

Figure 1.3: *Illustration of the possible position of a target (green) in 2D with measurements from two receivers.*

This can then be expanded to 3D. Using the same type of argument as above, then it is highly likely that the intersected "bubble", between the two "beams" from the receivers, holds the target. An illustration of this can be seen in Figure 1.4.

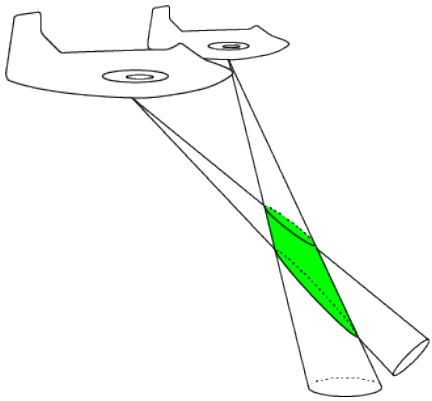

Figure 1.4: *Illustration of the possible position of a target (green) in 3D with measurements from two receivers.*

1.4 Terrain Data

In some scenarios, the elevation of the terrain is available. For one receiver, when the two angles are combined, then the position could be estimated to be within a certain area by projecting it down on a plane, see Figure 1.5. If $x = (x_1, x_2, x_3)^T$ is the static position of the target, where x_1 and x_2 are the lateral position and x_3 is the height, then with the available terrain data the height can be said to be a function of x_1 and x_2, or rather $x_3(x_1, x_2)$.

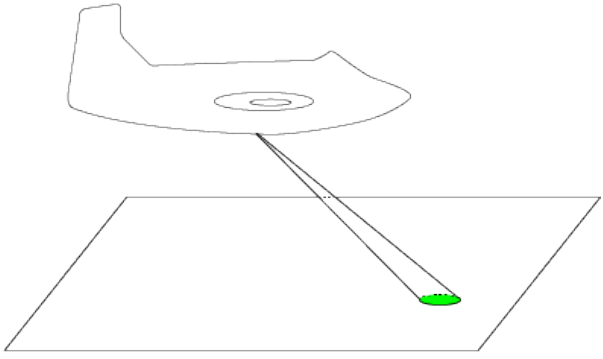

Figure 1.5: *Illustration of the target's possible position within a certain range (green) when combining with bearing measurements and terrain data.*

1.5 Limitations

Some relevant questions that are not considered in this thesis are for example path planning, detection of targets and cancellation of the methods when the targets are out of reach. The path planning is very relevant for either searching a certain area completely or following a target to not lose track of it. Path planning will not be used as the localization will be seen as a secondary task and the receivers primary goal is to get to a certain place instead of searching a certain area. Furthermore, the initialization and the cancellation are not considered, i. e., the localization system does not decide when the targets are within readable distance. It is assumed that another system activates the localization when the targets are detected and then cancel the system when the targets are out of range.

1.6 Related Problems

There are a lot of related problems to the airborne angle-only localization problem. Here, a short summary of jammers is presented as well as a short discussion of existing angle-only localization and tracking techniques. Lastly, there are a few words about SAR as it is a similar problem.

1.6.1 Jammers

In systems with wireless communication there is always a threat of interference, which could be intentional or unintentional. Commonly, when the interference is deliberate and has malicious intent, the devices are known as jammers. There are many different kinds of jammers for different purposes. In Xu et al. (2005), a few different jammer models are tested, such as a constant jammer, a deceptive jammer, a random jammer and a reactive jammer. The different kinds of jammers have different types of signals and therefore many of them may require different solutions to the detection, localization and tracking problems.

For a single target, there are a lot of scenarios that have been investigated. There are cases where there is only one airborne receiver that tracks a target (Ristic and Arulampalam, 2003), as well as when there is a fleet of UAVs that track a target (Bhamidipati and Gao, 2019; Koohifar et al., 2017). Other cases have used an array of static receivers and a static jammer (Joo and Sin, 2018) or a jammer in a moving car (Mitch et al., 2012).

With multiple targets, new problems arise. One problem is the data association problem which stems from the difficulty of separating the different measurements from each other. As the measurements from the different targets could get merged, the problem is to separate these measurements and connect them to the right target. It becomes even more difficult if the number of targets are unknown. This depends, however, often how close together the targets are. Some begin by estimating the number of jammers by a non-linear Gaussian-Mixture Probability Hypothesis Density (GM-PHD) filter (Bhamidipati and Gao, 2019) or

by Multiple Signal Classification (MUSIC) (Oispuu and Schikora, 2011; Schmidt, 1986). Then the localization can be done with a multiple methods, for example; power difference of arrival (PDOA) (Nyström, 2017), time difference of arrival (TDOA) (Bhatti et al., 2012; Nyström, 2017; Wang et al., 2010), maximum likelihood (ML) (Oispuu and Schikora, 2011), extended Kalman filter (EKF) (Oispuu and Schikora, 2011) and Graph-SLAM (Bhamidipati and Gao, 2019). The basis of many of these algorithms are explained in Bar-Shalom and Li (1993) and/or Gustafsson (2018).

1.6.2 Angle-Only Localization and Tracking

Angle-only tracking is very similar to the problem at hand and it has been investigate multiple times. The difference between tracking and localization is how the target's position is used over a time period. Tracking uses an adaptive estimation of the target's position, while localization does not. For angle-only tracking, different filtering techniques have been investigated and some solutions can be found in Aidala and Hammel (1983); Datta Gupta et al. (2015); Erlandsson (2007); Mehrjouyan and Alfi (2019); Ristic and Arulampalam (2003).

Other bearing-only problems are in principle the same type of problems as the localization of jammers with bearing-only measurements. In Erlandsson (2007) the author investigates filters for tracking an airborne target for collision avoidance and in Ristic and Arulampalam (2003) a general angle-only tracking problem is investigated. As it is possible to attach a jammer on to a UAV or a vehicle, the problem becomes the same for localization and tracking, but the solution could be used for different purposes.

For general angle-only localization problems, the methods could be implemented using either a batch of measurements or updating for every new sample. For example, Vaghefi et al. (2010) solves the same kind of general angle-only localization problem as this thesis but with different batch-wise least squares algorithms.

1.6.3 Search and Rescue

Another related problem is SAR, which is very similar to localization of jammers. In both problems the aim is to find a static target, often from an AV. The difference between SAR problems and interference problems is that finding the interference might be a secondary task, while, for SAR problems, finding and rescuing people is its highest priority. This can affect how the search is made, as the search mission might improve by, for example, path planning and area search planning.

1.7 Thesis Outline

This thesis is organized as follows. Firstly, some theoretical background is given in Chapter 2 where the mathematical formulation and its issues are presented to be able to understand the problem at hand. Secondly, the methods solving the

problem is presented in Chapter 3 and how to evaluate those methods in Chapter 4. Chapter 4 is divided into three parts where the first part discusses how the methods can be evaluated against a theoretical lower bound. There is also a discussion of when the lower bound exists and about parameter observability when elevation data is available. To see some results, a simple simulation system is implemented with more information in Section 4.2 where also the simulation scenarios are presented. The result of these simulation scenarios is then presented in Section 4.3. Lastly, there is an additional discussion and a conclusion in Chapter 5 and Chapter 6.

2

Theoretical Background

This chapter explores the mathematical formulation of the problem and explains the notation used throughout the thesis. As this is not the first time that bearing measurements have been used, some background information about their issues is talked about and how they can be avoided.

2.1 Mathematical Formulation

The problem can be described as finding the geographic position of the target from the azimuth angle, $\alpha \in [-\pi, \pi)$, and the elevation angle, $\epsilon \in [0, \pi/2)$, which the receiver measures in some way. Let the position of the target relative to the receiver be x_r with the nonstationary Cartesian coordinate system in Figure 2.1. If the relative target position is $x_r = (x_{r_1}, x_{r_2}, x_{r_3})^T$, then the bearing can be seen as a function of the position, which can be derived geometrically as:

$$\begin{pmatrix} \alpha(x_r) \\ \epsilon(x_r) \end{pmatrix} = \begin{pmatrix} \arctan2(x_{r_2}, x_{r_1}) \\ \arctan2(-x_{r_3}, \sqrt{x_{r_1}^2 + x_{r_2}^2}) \end{pmatrix} \tag{2.1}$$

The function "arctan2" is here an extended version of arctan where it is defined in all four quadrants, $-\pi \leq \arctan2(\cdot) \leq \pi$. This type of coordinate system is moving, as the receiver is assumed to be in flight. It should be noted that the target cannot be in the near proximity of the elevation angle $\pi/2$ because then the azimuth angle would be difficult to determine. This could be solved by using *quaternions*. However, if the elevation angle converges to $\pi/2$ then it is fairly certain that the target's position is directly below the receiver if the azimuth angle is difficult to determine. Therefore, one extra restriction is added where the target cannot be in the near proximity of the elevation angle $\pi/2$.

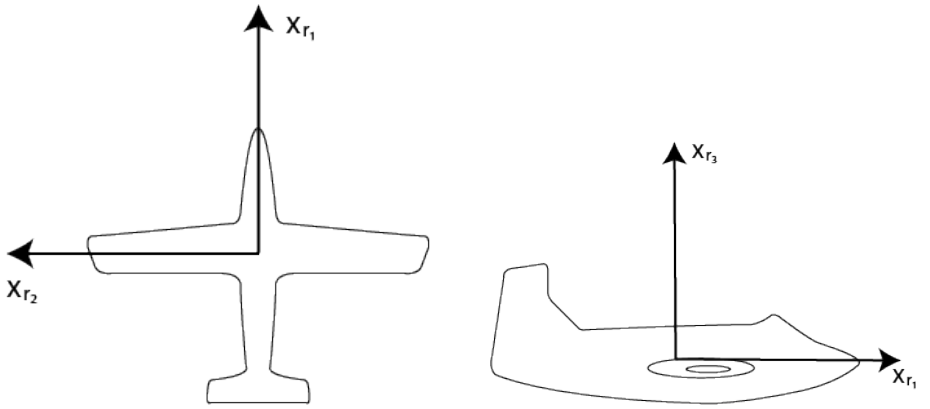

(a) From above. *(b)* From the side.

Figure 2.1: *The mobile Cartesian coordinate system with its origin in the receiver.*

By deciding on a global and static coordinate system, it is easier to relate every sample disregarding that there are multiple receivers. Let $y = (y_1, y_2, y_3)^T$ be the coordinates and $q = (\phi, \theta, \psi)^T$ be the roll, pitch and the yaw angle for an AV as well as let $x = (x_1, x_2, x_3)^T$ be the coordinates for the target in a global coordinate system. The setup of this global coordinate system is illustrated in Figure 2.2 for some global static coordinate system.

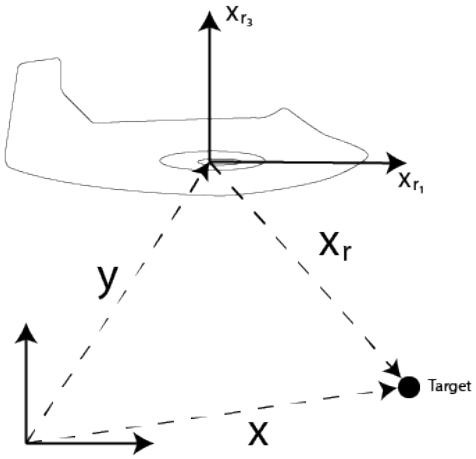

Figure 2.2: *The relation between the global coordinate system and the AV as well as the target.*

An illustration of the orientation of the AV, namely the yaw, pitch and roll angles, can be found in Figure 2.3. As the orientation of the AV influences the bearing,

let the rotation matrices for the roll, pitch and yaw angles be defined as (2.2). It is using the Euler angle representation to describe the rotation of the receivers coordinate system with respect to the stationary coordinate system.

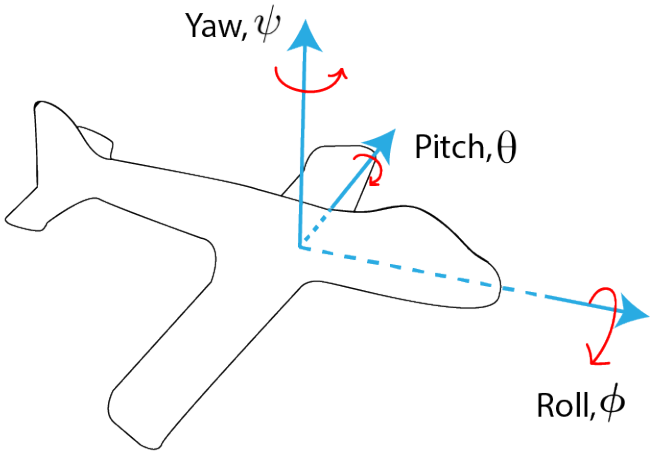

Figure 2.3: *The yaw (ψ), pitch (ϕ), and roll (θ) angles.*

$$\mathbf{R}_x(\phi) = \begin{bmatrix} 1 & 0 & 0 \\ 0 & \cos(\phi) & \sin(\phi) \\ 0 & -\sin(\phi) & \cos(\phi) \end{bmatrix} \tag{2.2a}$$

$$\mathbf{R}_y(\theta) = \begin{bmatrix} \cos(\theta) & 0 & -\sin(\theta) \\ 0 & 1 & 0 \\ \sin(\theta) & 0 & \cos(\theta) \end{bmatrix} \tag{2.2b}$$

$$\mathbf{R}_z(\psi) = \begin{bmatrix} \cos(\psi) & \sin(\psi) & 0 \\ -\sin(\psi) & \cos(\psi) & 0 \\ 0 & 0 & 1 \end{bmatrix} \tag{2.2c}$$

These individual rotation matrices can then be combined into one (c=cos and s=sin for simplicity):

$$\begin{aligned} \mathbf{R}(q) &= \mathbf{R}_x(\phi)\mathbf{R}_y(\theta)\mathbf{R}_z(\psi) \\ &= \begin{bmatrix} \mathrm{c}(\theta)\mathrm{c}(\psi) & \mathrm{c}(\theta)\mathrm{s}(\psi) & -\mathrm{s}(\theta) \\ \mathrm{s}(\theta)\mathrm{s}(\phi)\mathrm{c}(\psi)-\mathrm{c}(\phi)\mathrm{s}(\psi) & \mathrm{s}(\theta)\mathrm{s}(\phi)\mathrm{s}(\psi)+\mathrm{c}(\phi)\mathrm{c}(\psi) & \mathrm{c}(\theta)\mathrm{s}(\phi) \\ \mathrm{s}(\theta)\mathrm{c}(\phi)\mathrm{c}(\psi)+\mathrm{s}(\phi)\mathrm{s}(\psi) & \mathrm{s}(\theta)\mathrm{c}(\phi)\mathrm{s}(\psi)-\mathrm{s}(\phi)\mathrm{c}(\psi) & \mathrm{c}(\theta)\mathrm{c}(\phi) \end{bmatrix} \end{aligned} \tag{2.3}$$

Then the function of the angles in the moving coordinate system in (2.1) can be

written in a global coordinate system as

$$\begin{pmatrix} \alpha(\mathbf{R}(q)[x-y]) \\ \epsilon(\mathbf{R}(q)[x-y]) \end{pmatrix} \tag{2.4}$$

for some static global coordinate system. It should be noted that the target is static, which makes x a fixed point, while the AV has a motion with moving coordinates $y(t)$ and orientation $q(t)$.

The measurements are affected by additive noise $e(t)$, hence the angle measurements are written as

$$z(t) = \begin{pmatrix} \alpha(\mathbf{R}(q(t))[x-y(t)]) \\ \epsilon(\mathbf{R}(q(t))[x-y(t)]) \end{pmatrix} + e(t) \tag{2.5}$$

which is a nonlinear model where x should be estimated from the measured angles $z(t)$, the receiver position $y(t)$ and the orientation $q(t)$. The measurement error is assumed to be white Gaussian noise (WGN). Further information about WGN can be found in, for example, Olofsson (2011) or other books containing signal theory.

2.2 Notation

As the methods will be implemented in discrete time, let T be the sampling time and k be the k-th sample where $k = 0, 1, 2, ..., N-1$. Then a time changing variable, for example $q(t)$, will be sampled as

$$q(t_k) = q(kT) = q[k] = q_k$$

Sometimes an estimated quantity will be given the index $k|m$, e.g., $\hat{x}_{k|m}$. The indexation $k|m$ should be interpreted as *at time k given all the measurements up to, and including, time m*.

2.2.1 Measurement Function

The measurement function is given by

$$h(x,k) := h\Big(\mathbf{R}(q_k)(x-y_k)\Big) \tag{2.6}$$

where k denotes when the known signals, y_k and q_k, are measured. Both y_k and q_k are assumed to be known signals and they can be seen as a control signal/input. The definition in (2.6) can be used for both single and multiple receivers. If there are more than one receiver, the angle measurements are simply stacked as a column vector. For example, in case of two receivers the measurements are first the angles for receiver 1 and then the angles for receiver 2 which is shown in (2.7).

$$z_k = \begin{bmatrix} \alpha_k^1(x) \\ \epsilon_k^1(x) \\ \alpha_k^2(x) \\ \epsilon_k^2(x) \end{bmatrix} + e_k = h(x,k) + e_k \tag{2.7}$$

It should also be noted that the target's position, x, is calculated in 3D if there is no available elevation data and in 2D (lateral position) if elevation data is available. This stems from the knowledge of the terrain, which makes it unnecessary to calculate the height as it is already known for a certain lateral position.

In this project, the Jacobian is written as $J(x,k) = \nabla_x h(x,k)$ and the Hessian as $H(x,k) = \nabla_x^2 h(x,k)$. An approximation method for the Jacobian and Hessian is presented in Appendix A.1.

2.3 Issues with Angle-Only Measurements

The calculation of the bearing for radio frequencies has been developed over a long time, with one of the earliest works in 1943 using antenna arrays (Schelkunoff, 1943). Nowadays the antenna arrays might be distributed in several locations, on AVs or on cars, see for example Fei et al. (2020); Nyström (2017); Oispuu and Schikora (2011). There are also other methods of calculating the bearing, for example with an IR-sensor or radar, which subsequently can be used for localization or tracking (Schmidt, 1986). The main problems with angle-only measurements for static targets are

- *Observability*
- *Reflected Signals*

which will be discussed here after.

2.3.1 Observability

It was early understood that the receiver had to maneuver more than the target or have complementary measurements in order to have observability. This is easily illustrated by different paths of a moving target, as in Figure 2.4, where it is shown that different parallel paths can give rise to the same measurements in the receiver. In Fogel and Gavish (1988), they have derived the conditions for observability of the targets with Nth-order dynamic using angle measurements. The target's dynamic is its movement and they have concluded that the receivers have to make maneuvers with higher order dynamic than the target's for the target to be observable. Therefore, some movement from the receiver is needed to find stationary targets.

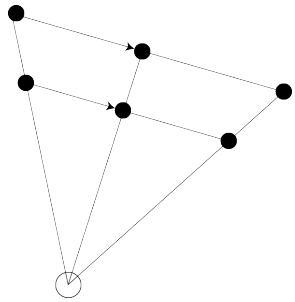

Figure 2.4: *A 2D example of an unobservable moving target and a static receiver. There are two target paths that could give the same measurements and therefore make the target unobservable. (• - target and ○ - receiver)*

Another 2D example of a not fully observable target can be seen in Figure 2.5 where two targets are aligned and static right in front of the AV. Both of the targets give the same measurements for a receiver moving towards them. For the targets to become distinguishable, the AV has to make a maneuver or have more information.

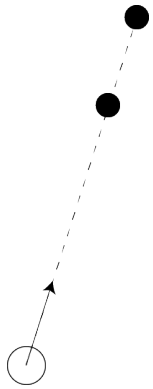

Figure 2.5: *A 2D example of unobservable targets for a moving receiver. (• - target and ○ - receiver)*

The definition of observability, according to Bar-Shalom and Li (1993), can be seen in Definition 2.1. For the system to be observable, the initial state (position of the target) should be uniquely recovered from the measurements. Therefore, it is very important for the system to be observable to obtain the estimation of the position, which is the goal.

Definition 2.1 (Observability). A continuous time system is completely observable if its initial state can be fully and uniquely recovered from its output, observed over a finite time interval, and the knowledge of the output.

2.3.2 Reflected Signals

In an area of mountains, for example, the original signal might bounce against the terrain before it goes towards the receiver. The reflected signal gives a lot more uncertainty than only a sensor measurement error. Therefore, the uncertainty of angle-only measurements can be greater depending on the terrain.

3

Localization Methods

There are numerous different localization methods that can be used for this problem. However, the ones used in this thesis are the nonlinear least squares (NLS), the extended Kalman filter (EKF) and the unscented Kalman filter (UKF). The most straight forward method is the nonlinear least squares (NLS). It optimizes a cost function and the argument, that gives the optimal solution, is the estimate. However, as it is difficult to calculate analytically, a numerical method is used. The algorithm used is a recursive nonlinear weighted least squares (NWLS) and it is chosen because it is a simple way to locate the target with short computation time. The next filter, the EKF, is chosen as it can handle the nonlinearity and it has a long history with different applications which makes it a well-tried filter. The UKF is chosen as a complement to the EKF and the NWLS as the UKF does not need any approximations of the derivatives, which both NWLS and EKF need.

All of these algorithms require an initial approximation of the position as well as an initial estimation of its covariance. The initialization problem and a method to handle it are presented in Section 3.3.

3.1 Nonlinear Weighted Least Squares

By seeing the position of the target as a parameter, then it is possible to estimate it by using nonlinear least squares (NLS). The NLS estimate is given by

$$\hat{x} = \arg\min_{x} V(x) \tag{3.1}$$

where $V(x)$ is the cost function and x is the position of the target (Gustafsson, 2018). Let $e_k(x) = z_k - h(x, k)$ and

$$\mathbf{e}_N(x) = (e_1^T(x), e_2^T(x), e_3^T(x), ..., e_N^T(x))^T$$

be the error from the measured angles for sample time 1 to N. Then the cost function is given by

$$V_N(x) = \frac{1}{2}\sum_{k=1}^{N} e_k^T(x)e_k(x) = \frac{1}{2}\mathbf{e}_N^T(x)\mathbf{e}_N(x) \tag{3.2}$$

This optimization might not be a simple task to solve as there could be multiple local optimums and/or the computing time might be large. A numerical optimization method might be preferred to make the optimization recursive. The nonlinear weighted least square is one such algorithm and one version of it is presented in Algorithm 1. It is based on the recursive linear weighted least squares (WLS) from Gustafsson (2018, pp. 510), but it uses the approximation $h(x,k) \approx J(x,k)x$.

Algorithm 1 Nonlinear Weighted Least Squares

Initialized with $\hat{x}_0$ and P_0.
Measurement update:

$$P_k = \left(P_{k-1}^{-1} + J^T(\hat{x}_{k-1},k)R^{-1}J(\hat{x}_{k-1},k)\right)^{-1}$$
$$\hat{x}_k = \hat{x}_{k-1} + P_k J^T(\hat{x}_{k-1},k)R^{-1}(z_k - h(\hat{x}_{k-1},k))$$

3.2 Kalman Filters

The Kalman filter (KF) has been used for many different purposes and also for localization and tracking. The KF updates the statistics recursively of a stochastic process to estimate the state. For linear Gaussian systems, the KF is the best possible state estimator. This means that the variance of the estimate is the minimum variance that can be achieved for a linear system. However, as this problem is nonlinear, the Kalman filter cannot be applied as it is. (Bar-Shalom and Li, 1993; Gustafsson, 2018)

A general system can be written as (3.3), where w and e are the process noise and the measurement noise, respectively. The variable x is the states to be estimated and z is the measurements. $f(\cdot)$ and $h(\cdot)$ are in general nonlinear functions. In this thesis, x is the position of the target and z is the measured angles, α and ϵ. As the position of the target is static, it is easy to conclude that $f(x_k,k) = x_k$. The function $h(x_k,k)$ is defined the same as in (2.7), and it is nonlinear. Furthermore, the measurement noise and process noise are assumed to be WGN with covariance matrices R and $Q(=0)$ respectively.

$$\begin{aligned} x_{k+1} &= f(x_k,k) + w_k \\ z_k &= h(x_k,k) + e_k \end{aligned} \tag{3.3}$$

To make the KF applicable to a nonlinear problem, there are a few different extensions that can be applied:

- *Extended Kalman Filter* (EKF): The Kalman filter can be expanded by using a Taylor expansion of the nonlinear function and linearize around the latest estimate. The EKF can handle the nonlinearity in the measurements and it has been used and tried for decades as well as it has low complexity.

- *Unscented Kalman Filter* (UKF): This filter utilizes the unscented transform for more accurate mapping from the state to the measurement using sigma points. It is a relatively new filter, presented in Julier et al. (1995), still it is widely used and it does not require derivations.

3.2.1 Extended Kalman Filter

The algorithm for the extended Kalman filter is stated in Algorithm 2. The function $\mathrm{tr}(\cdot)$ stands for the function *trace*, which is a sum of the diagonal elements.

Algorithm 2 Extended Kalman Filter (Gustafsson, 2018)

Initialized with $\hat{x}_{1|0}$ and $P_{1|0}$.
Measurement Update:

$$\begin{aligned} S_k &= R + J(\hat{x}_{k|k-1}, k)P_{k|k-1}J^T(\hat{x}_{k|k-1}, k) \\ &\quad + \frac{1}{2}\Big[\mathrm{tr}\Big(H_i(\hat{x}_{k|k-1}, k)P_{k|k-1}H_j(\hat{x}_{k|k-1}, k)P_{k|k-1}\Big)\Big]_{i,j} \end{aligned} \tag{3.4a}$$

$$K_k = P_{k|k-1}J^T(\hat{x}_{k|k-1}, k)S_k^{-1} \tag{3.4b}$$

$$\nu_k = z_k - h(\hat{x}_{k|k-1}, k) - \Big[\frac{1}{2}\mathrm{tr}(H_i(\hat{x}_{k|k-1}, k)P_{k|k-1})\Big]_i \tag{3.4c}$$

$$\hat{x}_{k|k} = \hat{x}_{k|k-1} + K_k\nu_k \tag{3.4d}$$

$$P_{k|k} = P_{k|k-1} - K_kS_kK_k^T \tag{3.4e}$$

Time Update:

$$\hat{x}_{k+1|k} = \hat{x}_{k|k} \tag{3.4f}$$

$$P_{k+1|k} = P_{k|k} + Q \tag{3.4g}$$

It should be noted that the EKF is a minimal mean square error (MMSE) estimator given that the earlier estimate $\hat{x}_{k|k-1}$ and the current measurement z_k are Gaussian random variables, according to Bar-Shalom and Li (1993) and Wan and Van Der Merwe (2000). However, the estimated measurement only uses an approximation of the distribution, which would not make this optimal. Furthermore, as this approximation is made only in one point, using the earlier estimate, then the mapping of the nonlinear function might not be as precise. An illustration of this

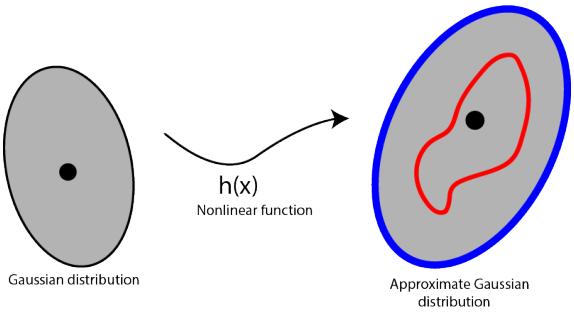

Figure 3.1: *An illustration of the real vs the approximated Gaussian of the measurement for the EKF. Blue-The best approximated Gaussian, Red-The actual Gaussian after using the nonlinear function, •-The mean.*

can be seen in Figure 3.1, where the approximated distribution does not necessarily look like the actual distribution. These imprecise approximations stem from its series expansion, which could introduce unmodeled errors. Although the EKF has its flaws, it is a useful filter since it is easy to work with. The initial estimation does not have to be perfect and neither does its initial covariance.

More details and information about the EKF can be found in, for example, Bar-Shalom and Li (1993), Gustafsson (2018) or Miller and Minkler (1993).

3.2.2 Unscented Kalman Filter

As the EKF only approximates the measurement using one point, another idea is to use many points by utilizing the unscented transform (UT). The UT uses the mapping of several sigma points in the belief that the approximation becomes better. In contrary to Figure 3.1, that describes the mapping of a distribution in the EKF, by adding sigma points the UT can be illustrated as Figure 3.2.

In the UT, the sigma points $\mathcal{X}$ of a variable x are calculated as (3.5), where μ_x is the mean of x, n_x is the dimension of x, λ is a composite scaling parameter and P is the covariance matrix of x. The index i in $(\sqrt{(n_x+\lambda)P})_i$ is the square root of the ith column of the matrix $(n_x+\lambda)P$. The square root can be calculated using singular value decomposition.

$$\mathcal{X}_0 = \mu_x, \tag{3.5a}$$

$$\mathcal{X}^i = \mu_x + (\sqrt{(n_x+\lambda)P})_i, \qquad i = 1, ..., n_x, \tag{3.5b}$$

$$\mathcal{X}^i = \mu_x - (\sqrt{(n_x+\lambda)P})_{i-n_x}, \qquad i = n_x+1, ..., 2n_x. \tag{3.5c}$$

The algorithm for the UKF is shown in Algorithm 3, where the UT is applied to an augmented state $x^a = [x^T, w^T, e^T]^T$ that includes the position of the target, the process noise and the measurement noise. The weights for the algorithm are calculated as in (3.6) with their design parameters presented in Table 3.1. In other

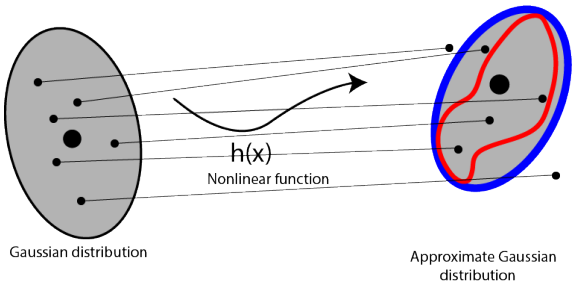

Figure 3.2: *An illustration of the real vs the approximated Gaussian of the measurement for the UKF. The lines are the mapping of sigma points. Blue-The best approximated Gaussian, Red-The actual Gaussian after using the nonlinear function,•-The mean.*

Table 3.1: *Design parameters for the unscented transform in the UKF. Chosen as in Wan and Van Der Merwe (2000) for Gaussian distributions.*

Parameter	Description	Value
a	Controls the spread of the sigma points.	10^{-3}
b	Incorporates prior knowledge of the distribution.	2
κ	Secondary scaling parameter.	0
λ	Scaling Parameter, $\lambda = a^2(n_a + \kappa) - n_a$.	$10^{-6}n_a - n_a$

UT literature, the parameters a and b are often written as α and β, however, they have been chosen this way to not confuse the reader with the azimuth angle. It should be noted that $\mathcal{Z}^i_{k|k-1}$ and $\hat{z}_{k|k-1}$ have been moved from the time update to the measurement update because the position and orientation of the receivers are known signals and they should be used with the current sample's measurements.

$$W_0^{(m)} = \frac{\lambda}{n_a + \lambda}, \tag{3.6a}$$

$$W_0^{(c)} = \frac{\lambda}{n_a + \lambda} + (1 - a^2 + b), \tag{3.6b}$$

$$W_i^{(m)} = W_i^{(c)} = \frac{1}{2(n_a + \lambda)}, \qquad i = 1, ..., 2n_a. \tag{3.6c}$$

Although, the UKF uses a lot of summations, the algorithm can be implemented with only matrix multiplications. There are more details of the UT and the UKF in Julier and Uhlmann (1997); Julier et al. (1995) and Wan and Van Der Merwe (2000).

Algorithm 3 Unscented Kalman Filter (Julier and Uhlmann, 1997)

Initialized with $\hat{x}_0$ and P_0.

Initialization:

$$\hat{x}^a_{0|0} = \begin{bmatrix} \hat{x}^T_0 & \mathbf{0} & \mathbf{0} \end{bmatrix}^T \tag{3.7a}$$

$$P^a_{0|0} = \begin{bmatrix} P_0 & \mathbf{0} & \mathbf{0} \\ \mathbf{0} & Q & \mathbf{0} \\ \mathbf{0} & \mathbf{0} & R \end{bmatrix} \tag{3.7b}$$

Calculate Sigma Points:

$$\mathcal{X}^a_{k|k} = \begin{bmatrix} \hat{x}^a_{k|k} & \hat{x}^a_{k|k} \pm \sqrt{(n_a + \lambda) P^a_{k|k}} \end{bmatrix}$$

Time Update:

$$\mathcal{X}^{x,i}_{k|k-1} = \mathcal{X}^{x,i}_{k-1|k-1} + \mathcal{X}^{w,i} \tag{3.7c}$$

$$\hat{x}_{k|k-1} = \sum_{i=0}^{2n_a} W^{(m)}_i \mathcal{X}^{x,i}_{k|k-1} \tag{3.7d}$$

$$P_{k|k-1} = \sum_{i=0}^{2n_a} W^{(c)}_i (\mathcal{X}^{x,i}_{k|k-1} - \hat{x}_{k|k-1})(\mathcal{X}^{x,i}_{k|k-1} - \hat{x}_{k|k-1})^T \tag{3.7e}$$

Measurements Update:

$$\mathcal{Z}^i_{k|k-1} = h(\mathcal{X}^{x,i}_{k|k-1}, k) + \mathcal{X}^{e,i} \tag{3.7f}$$

$$\hat{z}_{k|k-1} = \sum_{i=0}^{2n_a} W^{(m)}_i \mathcal{Z}^i_{k|k-1} \tag{3.7g}$$

$$S_k = \sum_{i=0}^{2n_a} W^{(c)}_i (\mathcal{Z}^i_{k|k-1} - \hat{z}_{k|k-1})(\mathcal{Z}^i_{k|k-1} - \hat{z}_{k|k-1})^T \tag{3.7h}$$

$$K_k = \Big(\sum_{i=0}^{2n_a} W^{(c)}_i (\mathcal{X}^{x,i}_{k|k-1} - \hat{x}_{k|k-1})(\mathcal{Z}^i_{k|k-1} - \hat{z}_{k|k-1})^T \Big) S_k^{-1} \tag{3.7i}$$

$$\hat{x}_{k|k} = \hat{x}_{k|k-1} + K_k(z_k - \hat{z}_{k|k-1}) \tag{3.7j}$$

$$P_{k|k} = P_{k|k-1} - K_k S_k K_k^T \tag{3.7k}$$

where $x^a = [x^T, w^T, e^T]^T$ is the augmented state, $\mathcal{X}^a = [(\mathcal{X}^x)^T, (\mathcal{X}^w)^T, (\mathcal{X}^e)^T]^T$ is the sigma points of the augmented state, λ is a scaling parameter, $n_a = \dim(x^a)$ and W_i is the weights, calculated as (3.6).

3.3 Initial Estimate and its Covariance

All methods require an initial estimate $\hat{x}_0$ and initial covariance P_0. In tracking, it is commonly calculated from the first sample or from the first couple of samples. Here, the initial estimate is calculated from the first sample.

The Gauss-Newton algorithm for nonlinear problems, presented in Algorithm 4, iterates the same sample until it finds a position that minimize the cost function from (3.2) or until certain conditions are met. The Gauss-Newton method for the NLS algorithm uses a few different parameters to terminate the search for new estimates. These parameters are described in Table 3.2.

Algorithm 4 Nonlinear Least Squares: Gauss-Newton (Gustafsson, 2018)

1. Set $i = 0$ and use a first approximation of $\hat{x}^{(0)}$ as input.
2. Set $a_i := 1$.
3. Calculate:
$$\hat{x}^{(i+1)} = \hat{x}^{(i)} + a_i\Big[J^T(\hat{x}^{(i)})R^{-1}J(\hat{x}^{(i)})\Big]^{-1}J^T(\hat{x}^{(i)})R^{-1}(z - h(\hat{x}^{(i)}))$$
4. **If** $V(\hat{x}^{(i+1)}) > V(\hat{x}^{(i)})$: Set $a_i := a_i/2$ and repeat from step 3.
5. **If** the *change in cost*, the *change in the estimate* or the *size of the gradient* is sufficiently small or if number of *max iterations* is reached: Terminate.
6. Set $i := i + 1$ and repeat from step 2.

The difficulty with the Gauss-Newton algorithm is its initialization. For a good initial estimate, the algorithm could converge very fast. However, if the initial estimate is bad then the algorithm can converge slowly, diverge or find a local minimum. (Constales et al., 2017)

For the initialization of the Gauss-Newton algorithm, there is an ad-hoc solution for this problem which is used only for this thesis. Assuming that the receiver has a range r where it can detect the target, it can take a few initial values from the circle created by that radius. If the points on the radius converge to the same point, while disregarding the diverging points, it becomes a good guess for an initial estimation.

The asymptotic covariance of a least-square estimate is given by (3.8a) (Huang et al., 2010), however, as it is a very optimistic estimation using only one sample instead of many, a larger covariance might be better. In this project, (3.8b) is used

instead.

$$P_0 = (J^T(\hat{x})R^{-1}J(\hat{x}))^{-1}, \tag{3.8a}$$

$$P_0 = 10^6\mathbf{I}. \tag{3.8b}$$

Table 3.2: *The parameters for the Gauss-Newton NLS algorithm.*

Parameter	Description	Value	Value (w. terrain data available)
ΔV	Discontinue the algorithm when the change of cost is sufficient small enough.	<1e-3	<1e-3
$\|\Delta\hat{x}\|_2$	Discontinue the algorithm when the change in estimate is sufficiently small enough.	<5m	<5m
$\|J^T(\hat{x}^{i+1})e(\hat{x}^{i+1}) - J^T(\hat{x}^i)e(\hat{x}^i)\|_2$	Discontinue the algorithm when the size of the gradient is sufficiently small enough.	<1e-2	<1e-4
max_iter	Max iterations before stopping the algorithm	10	10

3.4 Terrain Data Integration

For a certain lateral position it is possible to map the corresponding height from the terrain data, i.e. the height of a lateral position can be looked up. As the target's position is on ground level, this knowledge gives us the opportunity to disregard estimating the target's third dimension and instead focus on its lateral position. However, it cannot be disregarded altogether. The measurement function, $h(x, k)$, needs to have all three dimensions of the target to work properly, which is essential for all methods as well for the calculations of the Jacobian and the Hessian.

The target's height can be seen as a function of the lateral position, $x_3(x_1, x_2)$, and the target's position in three dimensions could be written as $x = [x_1, x_2, x_3(x_1, x_2)]^T$ for one sample. As the methods only calculates the lateral position, it influences the Jacobian and the Hessian as well. The derivatives are calculated only for two dimensions, instead of the usual three. All of this is illustrated in Figure 1.5 from

Section 1.4 as the terrain data acts like a plane which the bearing measurements projects down upon.

4

Experimental Evaluation

There are mainly two ways to evaluate the methods in Chapter 3; either by testing them on real data or by testing them on simulated data. By first simulating the problem, the solutions can be verified to work in a controlled environment before testing them on real data. As there is neither time nor resources to collect real data for this thesis, a simulation system is a great tool to evaluate the different methods.

This chapter is organized as follows. Section 4.1 describes how the methods can be evaluated empirically with simulations using Monte Carlo runs and how it can be compared to an analytical lower bound. It also discusses when there is parameter observability while using elevation data. How these simulations and simulation scenarios are implemented is shown in Section 4.2 with its simulated result presented in Section 4.3.

4.1 Performance Metrics

This section presents how the methods in Chapter 3 can be evaluated empirically with Monte Carlo simulations using the root mean square error (RMSE) and how it can be compared to the analytical lower bound, Cramér-Rao lower bound (CRLB). There is also an analysis of the analytical solution when elevation data is available, to see what assumptions or conditions have to be met for the target to be observable.

4.1.1 Performance Measures

When evaluating the performance of different filters, it could be advantageous to use a scalar measurement. One such measurement is the RMSE. It can be seen as

the standard deviation of the length of the estimated error. (Gustafsson, 2000)

One way to estimate the RMSE analytically is to use *Monte Carlo* simulations (runs). The Monte Carlo method makes many independent realizations/simulations to build up statistics. Let M be the number of independent realizations of the measurement z_k and j denote the jth realization. Then the measurement at time k for the jth simulation can be written as $z_k^{(j)}$. From $z_k^{(j)}$, different estimates of the position, $\hat{x}_t^{(j)}$, are made using the methods in Chapter 3 and they are compared to the true position, x_k^0, using the RMSE in (4.1). The superior index ^{0} signifies the true value and the subindex $_2$ represents the Euclidean norm.

$$\mathbf{RMSE}[k] = \left(\frac{1}{M} \sum_{j=1}^{M} \|\hat{x}_k^{(j)} - x_k^0\|_2^2 \right)^{1/2} \tag{4.1}$$

Note that the RMSE is time dependent. As the position of the target is not moving, it is also interesting to look at the whole data sequence as well. This gives an indication of how well the algorithm perform over an extended period of time. To make the RMSE for the whole sequence unbiased[1], the summation of the sequence is placed inside of the square, as in (4.2) (Gustafsson, 2000).

$$\mathbf{RMSE} = \left(\frac{1}{k} \sum_{i=1}^{k} \frac{1}{M} \sum_{j=1}^{M} \|\hat{x}_k^{(j)} - x_k^0\|_2^2 \right)^{1/2} \tag{4.2}$$

4.1.2 Cramér-Rao Lower Bound

Another interesting way to investigate the performance of the filters is to use the Cramér-Rao Lower Bound (CRLB). It is a theoretical lower bound for the covariance of an estimate. The closer the estimate's covariance is to the CRLB, the better the estimator. If the estimate's covariance reached the CRLB the estimator is said to be *efficient* Bar-Shalom and Li (1993). The CRLB for an unbiased estimator of the target's position x can be formulated as

$$\mathbf{E}\Big[(\hat{x} - x^0)(\hat{x} - x^0)^T\Big] = \mathrm{cov}(\hat{x}) \geq \mathcal{I}^{-1}(x^0) \tag{4.3}$$

where x^0 is the true value of x and $\mathcal{I}$ is the Fisher information matrix (FIM) (Bar-Shalom and Li, 1993; Gustafsson, 2018). The time index is dropped for simplicity. The FIM is defined as

$$\mathcal{I}(x) \triangleq \mathbf{E}\Big[\Big(\nabla_x \ln p(z|x)\Big)\Big(\nabla_x \ln p(z|x)\Big)^T\Big] \tag{4.4}$$

where $p(z|x)$ is the likelihood function (LF) which serves as a measure of how likely some observation z is, given a value of x (Bar-Shalom and Li, 1993; Gustafsson, 2018). The LF is calculated using the distribution of the measurement error

[1] Unbiased means that $\mathbf{E}[\hat{x}] = x^0$ where x^0 is the true value of x.

as in (4.5).

$$p(z|x) = p_e(z - h(x, u)) = \mathcal{N}(e(x); 0, R) \tag{4.5}$$

Using the Jacobian and that the error is Gaussian distributed, the FIM can be calculated as (4.6).

$$\ln p_e(e(x)) = -\frac{1}{2}\ln((2\pi)^N|R|) - \frac{1}{2}(e^T(x)R^{-1}e(x)) \tag{4.6a}$$

$$\nabla_x \ln p_e(e(x)) = J^T(x)R^{-1}e(x) \tag{4.6b}$$

$$\mathcal{I}(x) = \mathbf{E}\Big[J(x)^T R^{-1}e(x)(J^T(x)R^{-1}e(x))^T\Big] = J^T(x)R^{-1}J(x) \tag{4.6c}$$

For a static target without process noise, the information is assumed to be additive. The information is bound to increase monotonically with more information given. As it is assumed that two measurements are independent, then the current information can be calculated as the sum of the previous information and the added information. This is easily understood by considering the recursive CRLB formula of Algorithm 5.

Algorithm 5 Recursive Cramér-Rao Lower Bound

Initialized with $\mathcal{I}_0 = \mathbf{0}$.
Measurement update:

$$\mathcal{I}_k = \mathcal{I}_{k-1} + J^T(x_k^0, k)R^{-1}J(x_k^0, k)$$
$$P_k^{\text{CRLB}} = \mathcal{I}_k^{-1}$$

It is quite easy to compare the localization methods to the theoretical lower bound. The connection from CRLB to RMSE is as (4.7).

$$\mathbf{RMSE}[k] \geq \sqrt{\text{tr}(P_k^{\text{CRLB}})} \tag{4.7}$$

4.1.3 Observability with Elevation Data

As the CRLB utilizes the inverse of the FIM, it is assumed that the inverse of $\mathcal{I}(x) = J(x)R^{-1}J^T(x)$ exists. The inverse is needed in order to gain parameter observability or, with other words, the ability to observe the target. If the FIM is singular, e.g., if some eigenvalues are zero, then the inverse and hence the CRLB does not exist. If the inverse does not exist, then the matrix has infinite eigenvalues which makes the lower bound nonexistent.

For one receiver and no available terrain data the object would become partially unobservable. This stems from that there are two measurements (azimuth and elevation) and the position is in 3D. With this, the algorithms need to set three variables from two equations and this would not correspond to a unique solution

for the first sample. However, using elevation data, the height can be seen as a function of the 2D position, $x_3(x_1, x_2)$, and a unique solution should be found, thus making it observable with existing inverse of the FIM. However, depending on the angles, azimuth and elevation, there might be unobservable points even while using the elevation data.

The calculation of the inverse of the FIM might become a bit more tricky with available elevation data. If you know the lateral position, you can easily calculate the height. However, even if mapping the lateral position to the height is possible, it might become a problem to calculate its derivative as the function is unknown (can a map have a corresponding function describing its terrain?). In practice, it is likely that the terrain data is a summarized as a grid. This grid can be seen as a surface which could be approximated with a function. Still, this function could be as difficult to describe completely as the *true* terrain.

Let us examine the information $\mathcal{I}(x) = J^T(x)R^{-1}J(x)$ and $J(x) = \nabla_x h(x)$ with elevation data for one receiver. For simplicity, the time index k is dropped, which could be seen as a special case with $k = 1$. For shorter expressions, the position of the target is in the receiver's moving coordinate system, x_r. As the function of the terrain is unknown, let it be approximated as a plane as in (4.8) with $A, B, C \in \mathbb{R}$.

$$x_{r_3}(x_{r_1}, x_{r_2}) = Ax_{r_1} + Bx_{r_2} + C \tag{4.8}$$

This means that x_{r_3} now instead is a function. The relation between the angles and x_r can be seen in (4.9).

$$h(x_r) = \begin{pmatrix} \alpha(x_r) \\ \epsilon(x_r) \end{pmatrix} = \begin{pmatrix} \operatorname{arctan2}(x_{r_2}, x_{r_1}) \\ \operatorname{arctan2}(-(Ax_{r_1} + Bx_{r_2} + C), \sqrt{x_{r_1}^2 + x_{r_2}^2}) \end{pmatrix} \tag{4.9}$$

The derivatives of the angles are stated in (4.10) and the calculations for them can be found in Appendix A.2.

$$\frac{\partial \alpha}{\partial x_{r_1}} = \frac{-x_{r_2}}{x_{r_1}^2 + x_{r_2}^2} \tag{4.10a}$$

$$\frac{\partial \alpha}{\partial x_{r_2}} = \frac{x_{r_1}}{x_{r_1}^2 + x_{r_2}^2} \tag{4.10b}$$

$$\frac{\partial \epsilon}{\partial x_{r_1}} = (x_{r_1}^2 + x_{r_2}^2)^{-1/2} \frac{Bx_{r_1}x_{r_2} + Cx_{r_1} - Ax_{r_2}^2}{x_{r_1}^2 + x_{r_2}^2 + (Ax_{r_1} + Bx_{r_2} + C)^2} \tag{4.10c}$$

$$\frac{\partial \epsilon}{\partial x_{r_2}} = (x_{r_1}^2 + x_{r_2}^2)^{-1/2} \frac{Ax_{r_1}x_{r_2} + Cx_{r_2} - Bx_{r_1}^2}{x_{r_1}^2 + x_{r_2}^2 + (Ax_{r_1} + Bx_{r_2} + C)^2} \tag{4.10d}$$

The Jacobian is defined as (4.11) and it is, in this simple case, a square matrix. For invertible matrices $J(x)$ and R then $[J^T(x)R^{-1}J(x)]^{-1} = J^{-1}(x)RJ^{-T}(x)$ must be

true.

$$J(x_r) = \frac{\partial}{\partial x_r} h(x_r) = \begin{bmatrix} \frac{\partial \alpha}{\partial x_{r_1}} & \frac{\partial \alpha}{\partial x_{r_2}} \\ \frac{\partial \epsilon}{\partial x_{r_1}} & \frac{\partial \epsilon}{\partial x_{r_2}} \end{bmatrix} \tag{4.11}$$

The Jacobian is invertible if and only if it has full rank. Therefore, let us take a look at its determinant and when it is equal to zero:

$$\begin{aligned} 0 &= \frac{\partial \alpha}{\partial x_{r_1}} \frac{\partial \epsilon}{\partial x_{r_2}} - \frac{\partial \alpha}{\partial x_{r_2}} \frac{\partial \epsilon}{\partial x_{r_1}} \\ &\implies \\ 0 &= -x_{r_2}(A x_{r_1} x_{r_2} + C x_{r_2} - B x_{r_1}^2) - x_{r_1}(B x_{r_1} x_{r_2} + C x_{r_1} - A x_{r_2}^2) \\ &= \cancel{-A x_{r_1} x_{r_2}^2} - C x_{r_2}^2 + \cancel{B x_{r_1}^2 x_{r_2}} - \cancel{B x_{r_1}^2 x_{r_2}} - C x_{r_1}^2 + \cancel{A x_{r_1} x_{r_2}^2} \\ &= -C(x_{r_1}^2 + x_{r_2}^2) \end{aligned}$$

Thus, for the Jacobian to have full rank then $0 \neq -C(x_{r_1}^2 + x_{r_2}^2)$. There are two cases where the inverse of the Jacobian does not exist; $C = 0$ and $x_{r_1} = x_{r_2} = 0$. The singularity from $x_{r_1} = x_{r_2} = 0$ stems from the origin of the problem itself. When the elevation angle is $\pi/2$, then the object is right below the receiver and the azimuth angle can take any value without changing this fact. As the azimuth can take on any value, it makes the object unobservable. However, from this fact, an operator/pilot can come to the conclusion that the target is directly below but with unknown statistical accuracy.

It should be noted that the orientation of the receiver is important as x_r is the relative position of the target. If the receiver makes a maneuver, its coordinate system rotates and then this singularity might not be directly below the receiver. This only becomes a problem when the receiver faces the target with its belly.

It is also problematic when $C = 0$ which means that at least a constant height difference has to exist for the Jacobian to exist. As it is assumed that the target is on the ground and that the receiver is an AV, the assumption that there is at least a constant height difference C is reasonable. If the target has the same height as the receiver but is also on the ground, then those facts are contradicting each other. If this occurs in a mountainous area, then an operator/pilot could make the assumption that the target is on a mountain.

4.2 Implementation and Simulation Specifications

This section presents the parameters and their values for a simple simulation system as well as illustrate the different simulation scenarios.

4.2.1 Simulations

To evaluate the methods, a simple simulation system is implemented in MATLAB. The general parameters for the simulation and their value are stated in Table 4.1. Every scenario is simulated with 1000 Monte Carlo runs to gain somewhat accurate statistics. The measurement covariance, in all receivers, is given by

$$R = \begin{bmatrix} \sigma_e^2 & 0 \\ 0 & \sigma_e^2 \end{bmatrix} \tag{4.12}$$

where, following the discussion of Gustafsson (2018, p. 404), $\sigma_e \in [5°, 10°]$ is assumed. Therefore, some investigation will be done on both 5°and 10°to see how the methods behave for the different extremes of the standard deviation. The movement of the receivers is based on uniform motion, where the receivers continue forwards with a constant velocity.

Table 4.1: *Parameters for simulation.*

Parameter	Description	Value	Unit
T	Sample time	0.1	s
M	Number of simulations	1000	-
σ_e	Standard deviation of measurement noise	5 or 10	°
Δ	Offset for approximation of the Jacobian and Hessian	50	m

4.2.2 Elevation Data

The terrain data available is an elevation data grid with grid size 50m×50m from *Elevation data, grid 50+ © Lantmäteriet* (Lantmäteriet). It is based on the national elevation model and it has an average fault of 1m. However, this can be much higher for hilly terrain. The data is collected and maintained with laser data as well as use measurement of changes in aerial images. The national elevation model is based on an one meter grid which is interpolated with a bilinear method a couple of times until it reaches a 50 meter grid. For this project, it is assumed that the height is correct for flatter areas.

4.2.3 Scenarios

There are two flight paths that will be investigated in this thesis. The different paths have been chosen to get two geometrically different problems. Let the first

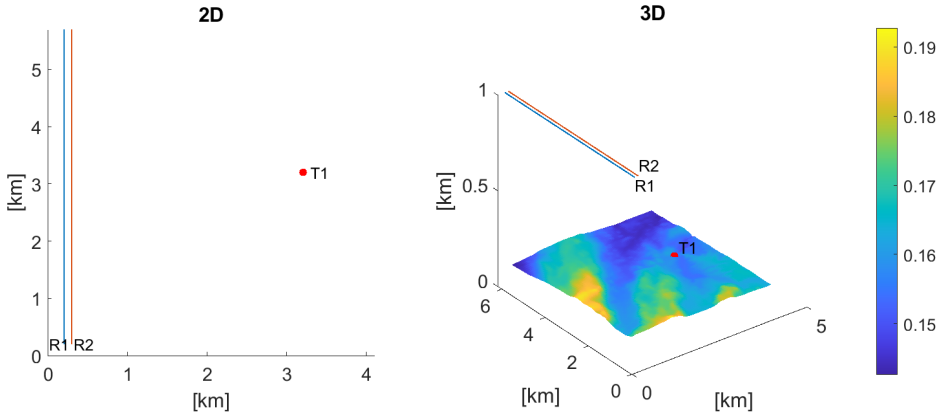

(a) *2D view of the path from above.*

(b) *3D view of the path where the height data is colored. The light/yellow parts are higher up than the lower blue parts. Elevation data, grid 50+ © Lantmäteriet*

Figure 4.1: *The parallel flight path.*

flight path be called *parallel*, see Figure 4.1. There are two AVs that fly 100 meters apart in *parallel* and the paths are straight. The target is a few kilometers away and the terrain is mostly flat. The receivers' initial positions and velocities can be found in Table 4.2.

Table 4.2: *Parameters for the parallel flight path.*

Parameter	Description	Value	Unit
x	Target position	$(3.2, 3.2, 0.154)^T$	km
$y^{(1)}$	Receiver 1 initial position	$(0.2, 0.2, 1)^T$	km
$y^{(2)}$	Receiver 2 initial position	$(0.3, 0.2, 1)^T$	km
v	Velocity of the receivers	200	m/s

The other flight path that will be investigated is illustrated in Figure 4.2 and it is called *crossed*. This name stems from the direction of the individual flight paths of the receivers. Their flight paths are straight but perpendicular to each other. The starting psoitions and velocities are found in Table 4.3.

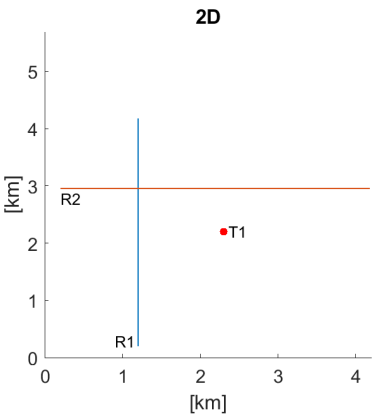

(a) 2D view of the path from above.

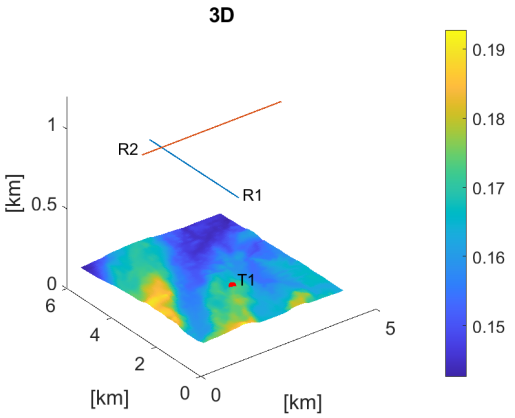

(b) 3D view of the path where the height data is colored. The light/yellow parts are higher up than the lower blue parts. Elevation data, grid 50+ © Lantmäteriet

Figure 4.2: *The crossed flight path.*

Table 4.3: *Parameters for the crossed flight path.*

Parameter	Description	Value	Unit
x	Target position	$(2.2, 2.2, 0.172)^T$	km
$y^{(1)}$	Receiver 1 initial position	$(1.1, 0.2, 1)^T$	km
$y^{(2)}$	Receiver 2 initial position	$(0.1, 2.95, 1.1)^T$	km
v	Velocity of the receivers	200	m/s

The scenarios are chosen in this way as it is hypothesized that the parallel flight path gives less information than the crossed flight path. As the two receivers in parallel receive almost the same measurements, then it is assumed that the information gained by the extra receiver is small. For the crossed, however, there could be more gain as each sample could give more information.

There are five scenarios that will be investigated. The summary of what each scenario includes can be found in Table 4.4. The difference between each scenario can be the number of receivers, the flight path or if elevation data is available.

Table 4.4: *Summary of the different scenarios.*

Scenario	Targets	Receivers	Flight path	Elevation data
1	1	2	Parallel	Not available
2	1	2	Parallel	Available
3	1	1 (only R1)	Parallel	Available
4	1	2	Crossed	Not available
5	1	2	Crossed	Available

The different scenarios were chosen as they all have different information, even if the flight path is the same. For example, scenario 2 has more information than scenario 1 as elevation data is available. However, comparing these two scenarios might be unfair, due to the difference in available information. Therefore another scenario was added. In scenario 3, one receiver is removed to decrease the amount of information extracted.

4.3 Results

This chapter is divided into two parts where the first part presents the results for the parallel flight path and the second part presents the results for the crossed flight path. The evaluation method is the same as presented in Section 4.1, where the estimated standard deviation of the target's position plays a heavy part. It is calculated by the RMSE and it is compared to the CRLB. The CRLB is the theoretical lower bound that the RMSE can achieve. Therefore, if the RMSE is close to the CRLB, it is difficult to get any better results, and hence the estimator performs well in the specific problem.

The RMSE and CRLB are calculated only for the lateral position, even if some scenarios also estimate the height of the target. It is because it is easier to compare the different scenarios and their values if they compare the same parameters.

4.3.1 Parallel Flight Path

The RMSE of the target's position for scenario 1-3 can be found in Figure 4.3. The standard deviation of the measurement error is $\sigma_e = 10°$ for all scenarios. In Figure 4.3a, the RMSE for scenario 1 is shown. It takes $\gtrapprox 12$ seconds for the methods to flatten their curves and the majority of the time the EKF is clearly lower than either NLS and UKF. There is no method that is close to the CRLB for an extended period of time.

Scenario 2 is given by adding the elevation data and the RMSE curves are found in Figure 4.3b. The knowledge of the terrain lowers the RMSE towards the CRLB and all of the methods have similar curves. From ≈ 15 seconds, it seems like all methods are approximately the same as the CRLB. Removing one receiver for scenario 3, the RMSE is given by Figure 4.3c. The graph for scenario 3 is similar to scenario 2, however, it is not as steep in the first 10 seconds.

In roughly the first second of Figure 4.3c the methods are below the CRLB, which is quite surprising. Still, this could be explained by the initialization. As the initialization use the assumption that the receiver can detect a target within a certain range, the localization could be slightly better in the beginning.

To see which method perform better over time, let us look at the RMSE for the whole data sequence, which is shown in Table 4.5. In scenario 1, the EKF has much lower RMSE than the others. While for scenario 2 and 3, the NLS perform slightly better than both the EKF and the UKF. All methods converge, sooner or later, to the CRLB except for the NLS and UKF in scenario 1. Furthermore, the convergence is slower for EKF in scenario 1.

For $\sigma_e = 5°$ and $\sigma_e = 10°$, the methods give similar graphs respectively for every scenario. One example is scenario 1, which is shown in Figure 4.4. All methods have similar appearance for both σ_e and the curves of the methods have compa-

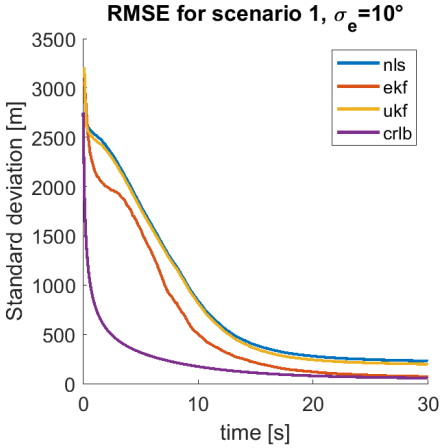

(a) Scenario 1: Two receivers and no available elevation data.

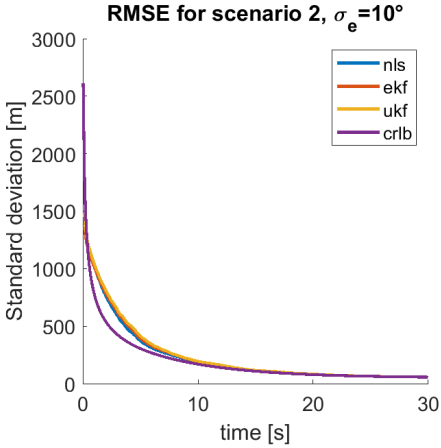

(b) Scenario 2: Two receivers and available elevation data.

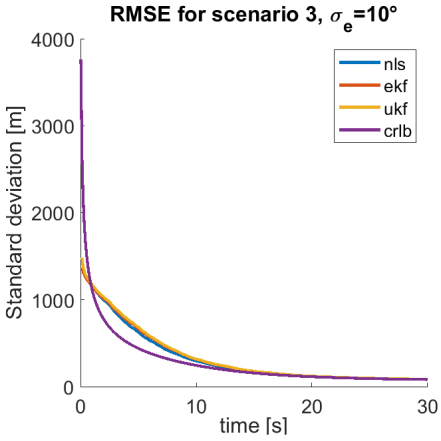

(c) Scenario 3: One receiver and available elevation data.

Figure 4.3: *The estimated standard deviation of the target's position compared to the CRLB for the parallel flight path. $\sigma_e = 10°$.*

Table 4.5: *Comparison between the RMSE and CRLB for the whole sequence for different standard deviations of the measurement error (parallel flight path).*

Scenario	σ_e	**RMSE** [m] (NLS)	**RMSE** [m] (EKF)	**RMSE** [m] (UKF)	CRLB [m]
1	5°	950	756	925	155
1	10°	1126	939	1105	310
2	5°	176	177	183	148
2	10°	346	349	362	297
3	5°	229	238	243	213
3	10°	449	459	469	427

rable shape. However, for smaller deviation, the methods converge faster with a steeper curve. For lower σ_e, the CRLB becomes lower as well.

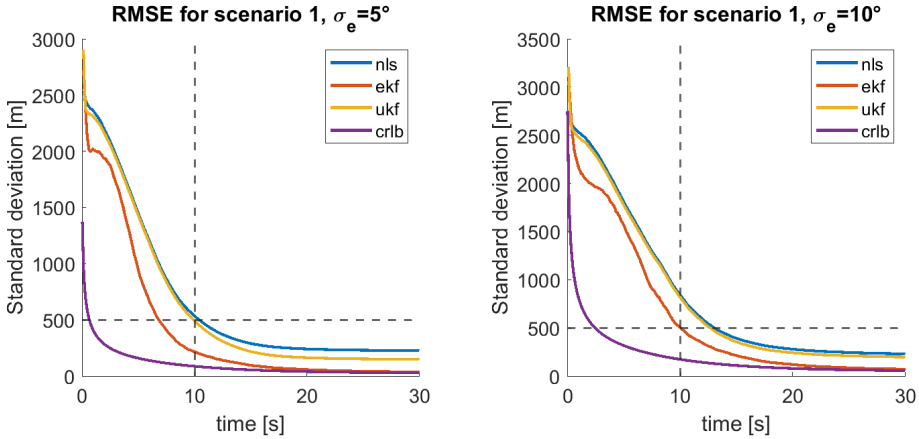

(a) $\sigma_e = 5°$. ***(b)*** $\sigma_e = 10°$.

Figure 4.4: *The estimated standard deviation compared to the CRLB for scenario 1 (parallel flight path).*

4.3.2 Crossed Flight Path

The RMSE of the target's position for scenario 4 and 5 can be found in Figure 4.5. The standard deviation of the measurement error is $\sigma_e = 10°$. Both scenarios give very similar graphs even though scenario 5 have more information as it has access to elevation data. The main difference between the scenarios is the first couple of seconds where both are distinguishable from the CRLB. With scenario 4 there are more uncertainty during that time, but it converges fast towards the lower bound.

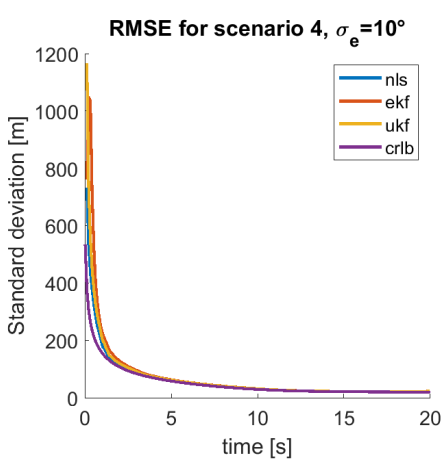

(a) Scenario 4: Two receivers and no available elevation data.

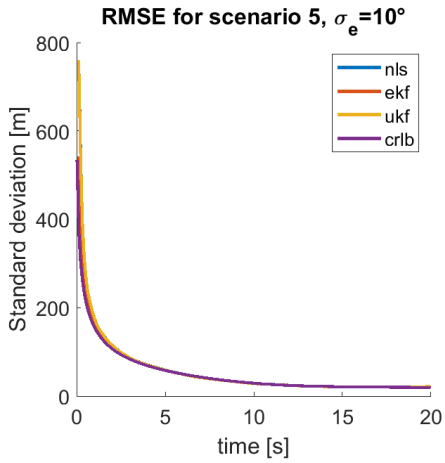

(b) Scenario 5: Two receivers and available elevation data.

Figure 4.5: *The estimated standard deviation of the target's position compared to the CRLB for the crossed flight path. $\sigma_e = 10°$.*

Table 4.6: *Comparison between the RMSE and CRLB for the whole sequence for different standard deviations of the measurement error (crossed flight path).*

Scenario	σ_e	**RMSE** [m] (NLS)	**RMSE** [m] (EKF)	**RMSE** [m] (UKF)	CRLB [m]
4	5°	46	110	71	36
4	10°	102	153	132	72
5	5°	57	45	57	36
5	10°	99	84	99	72

The information gained by the knowledge of the terrain seems to be small, as the all the methods converge quickly to the CRLB, which is the same for both scenarios. The main difference between the scenarios is the first couple of seconds where the RMSE is much higher for scenario 4. This can also be seen in in Table 4.6, where the majority of the methods are better for scenario 5 than scenario 4, while also being quite near the CRLB. For scenario 4, the NLS perform better than the other methods, however, for scenario 5 the EKF perform better.

5
Discussion

Looking at the simulation results it is fairly obvious that the relative flight paths of the receivers are very important. For different relative flight paths the receivers will generate measurements with different information content, which subsequently means that the estimation performance will differ. For the parallel flight path in scenario 1, all of the methods converge slowly or not at all to the CRLB, while for the corresponding scenario for the crossed flight path, scenario 4, the methods converge fast. As the two flight paths are two different problems, their numerical value is difficult to compare. However, their appearance and how quickly the converge tell us that the receivers' relative path is important for the results.

Nonetheless, the geometry of the problem is not as important if elevation data is available. Both scenario 2 and 5, which use two receivers and elevation data, converge fairly quickly to the CRLB. This could stem from that it is possible to locate the target using only one receiver when elevation data is available. Therefore, it can be said that the relative flight path is important to get good localization but it is not as critical when elevation data is available.

The measurement noise is also important for better results. With smaller σ_e, the methods perform better. Therefore, if the measurement error could be minimal, then the results would improve, independent of the method used.

The available elevation data is, in this case, restricted to Sweden and there are a few areas that are not covered and/or have missing data. For algorithms depending on the elevation data, this could be critical for the localization. If the data is not available, then the algorithms would cease to function properly. This could also be a problem for flying over new areas not covered in the data, for

example in a foreign country. It should also be noted that having too much data could also be problematic. A big data base needs a lot of memory space, which could be restricted for AVs.

The improvement of the methods between scenario 1 and 2, when the terrain data is added, is great. With elevation data, the RMSE can converge quicker towards the CRLB. This highlights the difficulty to determine the position using similar measurements. Conceptually, this could be explained with Figure 1.4 from Section 1.3, where "beams" from two receivers cross each other and they point out where the most likely position is within a volume. For two receivers which receive similar measurements, these "beams" overlap more volume than for receivers that receive very different measurements. Then when the elevation data is added, it restricts not only the possible height but also the lateral position.

Comparing scenario 2 and 3, the result is fairly similar in appearance to each other even if there is one receiver less in scenario 3. This could be interpreted as the extra receiver does not add much information when the AVs fly in parallel. However, looking at the RMSE for the whole data sequence, there is a significant difference in value between the two scenarios where scenario 2 is a lot less than scenario 3. The CRLB for scenario 3 is also much higher than scenario 2, which means that a lot could be gained by an extra receiver although the receivers get similar measurements.

Continuing with the RMSE for the whole sequence, there are not many meters that differ between the CRLB for scenario 1 and 2. Although, scenario 2 has elevation data, the CRLB for scenario 1 is only 13m higher than scenario 2. This could be compared to the CRLB for scenario 3 which is a lot higher than for either scenario 1 and 2. This implies that the information gained by knowing the environment is less than adding an extra receiver for this specific problem with this terrain data set, covariance and number of receivers.

Although it might be possible to have good results without elevation data, the RMSE for the parallel flight path shows a different story. All methods perform better in scenario 3 (one receiver, elevation data) compared to scenario 1 (two receivers). Therefore, the geometry of the problem is important to get good localization with two receivers while it is not as important when elevation data is available.

For more than one receiver, there is another problem that arises. For an update of the target's position in real-time, then the receivers have to communicate. However, the line of communication could be restricted. There might be a limit of how much information can be sent between two receivers and other communication might be more important than locating a jammer. Therefore, the user has to consider whether it is more reasonable to use two receivers that need to communicate or to use one receiver that use more memory space.

The individual methods give very similar results when elevation data is in use, independently of the scenario. There is not a clear advantage to chose one method over the others. The only advantage that exists when all methods perform similarly, is the computation time. The NLS has less computation time viewing at the calculations needed for every update. This, however, would not be noticeable for the user as all methods are fairly quick.

When there is no elevation data, the performance of the methods are different from each other. Here, the EKF stands out for scenario 1. It is the only method that converges to the CRLB and its RMSE is also lower than the other methods the majority of the time. Yet, for scenario 4 the EKF is the method that has the worst performance. Still, it converges quickly towards the CRLB following the NLS and the UKF. Here, the user has to do a trade-off to see what method is more advantageous to use for certain situations. It could either be 1.) having a method that always converges to CRLB, although it might be slow, or 2.) a method that only converges to CRLB sometimes, but when it does converge, it is better.

6

Conclusion

In summary, this thesis has introduced elevation data to the airborne angle-only geolocalization problem using three localization methods, the nonlinear least squares (NLS), the extended Kalman filter (EKF) and the unscented Kalman filter (UKF). These methods have been implemented with and without elevation data, and they have been compared to the Cramér-Rao Lower Bound (CRLB) to see if there are some advantages to use elevation data. There have also been a discussion of the observability when elevation data is in use.

With elevation data it can be said that the localization gives more consistent results independently of the method used or the geometry of the problem. All methods converge fairly quickly to the CRLB when elevation data is available for the tried geometries in this thesis. However, for more than one receiver it might be unnecessary to use elevation data. If the measurements have enough information embedded then it does not matter if elevation data is added because the localization is almost as good with it as without it.

For multiple receivers, there is a need for a communication channel between the receivers. Thus, if there are multiple receivers available that can communicate while flying differently from each other, there is no need to add elevation data. Yet, if the receivers receive similar measurements to each other, the localization can significantly improve with elevation data. It is also noteworthy that the localization still works for one receiver when elevation data is accessible as it can eliminate the disadvantages of communication and planning of the relative flight path.

There is no method that is clearly better than the others when elevation data is available. The methods' performances are very similar but that could also be

an advantage. This makes the usage of elevation data not restricted to a certain method and it leaves more up to the implementer which method they prefer.

6.1 Future Work

For future work, it would be interesting to see how well the methods perform in real-life as this thesis only tried the scenarios with simulations. However, for real-life scenarios there might be different data available. For example, instead of azimuth and elevation there might only be azimuth measurements available or azimuth and RSS[1]. All these different combinations might be interesting to investigate with elevation data. Furthermore, the terrain could be different depending on location, which makes it engaging to see how well these methods perform for mountainous terrain. This is particularly interesting for, for example, search and rescue (SAR) for mountain rescue.

An immediate continuation of this thesis is to add movement to the target and make it a tracking problem. It is not unthinkable to put a jammer in, for example, a car. This problem could also include elevation data, to see if there is any improvement to the tracking with or without elevation data.

Another addition is to add more targets and to estimate the bearing measurements. For example, radio frequencies, which many jammers use, can interfere with each other and the bearing measurements is often calculated with antenna arrays. Thus, if the radio frequencies are modelled (or used in reality), it could be interesting to see how well the methods perform when the association problem arise and how the solutions presented in this thesis could be combined to a larger problem that is more similar to real life.

[1] Received Signal Strength.

Appendix

A

Derivatives

This chapter explains which numerical approximations are used for the Jacobian and Hessian as well as calculates the derivatives of azimuth and elevation in the receivers own coordinate system.

A.1 Numerical Approximation

A numerical approximation of the Jacobian and Hessian can be preferred if they are difficult to calculate by hand or if they are too complex which requires much computer code, memory or computational time. Using a forward difference of Δ, the Jacobian and Hessian can be approximated as (A.1), where the sub-indices i, j of Δ is the difference applied to a certain dimension. (Gustafsson, 2018)

$$\frac{\partial h(x)}{\partial x_i} \approx \frac{h(x + \Delta_i) - h(x)}{\Delta} \tag{A.1a}$$

$$\frac{\partial^2 h(x)}{\partial x_i \partial x_j} \approx \frac{1}{\Delta^2}\Big(h(x + \Delta_i + \Delta_j) - h(x + \Delta_i) - h(x + \Delta_j) + h(x)\Big) \tag{A.1b}$$

These approximations will be used for the Jacobian and Hessian used in the methods.

A.2 Azimuth and Elevation

Here are the calculations of the derivatives of the Azimuth and Elevation angles in the relative coordinate system. They are used in Section 4.1.3 to see where

there is observability.

$$\begin{aligned}\frac{\partial \alpha}{\partial x_{r_1}} &= \frac{1}{1+(\frac{x_{r_2}}{x_{r_1}})^2}\frac{\partial}{\partial x_{r_1}}\Big(\frac{x_{r_2}}{x_{r_1}}\Big)\\ &= \frac{1}{1+(\frac{x_{r_2}}{x_{r_1}})^2}\Big(-\frac{x_{r_2}}{x_{r_1}^2}\Big)\\ &= \frac{-x_{r_2}}{x_{r_1}^2+x_{r_2}^2}\end{aligned}$$

$$\begin{aligned}\frac{\partial \alpha}{\partial x_{r_2}} &= \frac{1}{1+(\frac{x_{r_2}}{x_{r_1}})^2}\frac{\partial}{\partial x_{r_2}}\Big(\frac{x_{r_2}}{x_{r_1}}\Big)\\ &= \frac{1}{1+(\frac{x_{r_2}}{x_{r_1}})^2}\Big(\frac{1}{x_{r_1}}\Big)\\ &= \frac{x_{r_1}}{x_{r_1}^2+x_{r_2}^2}\end{aligned}$$

$$\begin{aligned}\frac{\partial \epsilon}{\partial x_{r_1}} &= \frac{1}{1+(\frac{-x_{r_3}}{\sqrt{x_{r_1}^2+x_{r_2}^2}})^2}\frac{\partial}{\partial x_{r_1}}\Big(\frac{-x_{r_3}}{\sqrt{x_{r_1}^2+x_{r_2}^2}}\Big)\\ &= \frac{x_{r_1}^2+x_{r_2}^2}{x_{r_1}^2+x_{r_2}^2+(Ax_{r_1}+Bx_{r_2}+C)^2}\Big(\frac{x_{r_1}(Ax_{r_1}+Bx_{r_2}+C)}{(x_{r_1}^2+x_{r_2}^2)^{3/2}}-\frac{A}{\sqrt{x_{r_1}^2+x_{r_2}^2}}\Big)\\ &= (x_{r_1}^2+x_{r_2}^2)^{-1/2}\frac{\cancel{Ax_{r_1}^2}+Bx_{r_1}x_{r_2}+Cx_{r_1}-A(\cancel{x_{r_1}^2}+x_{r_2}^2)}{x_{r_1}^2+x_{r_2}^2+(Ax_{r_1}+Bx_{r_2}+C)^2}\\ &= (x_{r_1}^2+x_{r_2}^2)^{-1/2}\frac{Bx_{r_1}x_{r_2}+Cx_{r_1}-Ax_{r_2}^2}{x_{r_1}^2+x_{r_2}^2+(Ax_{r_1}+Bx_{r_2}+C)^2}\end{aligned}$$

$$\begin{aligned}\frac{\partial \epsilon}{\partial x_{r_2}} &= \frac{1}{1+(\frac{-x_{r_3}}{\sqrt{x_{r_1}^2+x_{r_2}^2}})^2}\frac{\partial}{\partial x_{r_2}}\Big(\frac{-x_{r_3}}{\sqrt{x_{r_1}^2+x_{r_2}^2}}\Big)\\ &= \frac{x_{r_1}^2+x_{r_2}^2}{x_{r_1}^2+x_{r_2}^2+(Ax_{r_1}+Bx_{r_2}+C)^2}\Big(\frac{x_{r_2}(Ax_{r_1}+Bx_{r_2}+C)}{(x_{r_1}^2+x_{r_2}^2)^{3/2}}-\frac{B}{\sqrt{x_{r_1}^2+x_{r_2}^2}}\Big)\\ &= (x_{r_1}^2+x_{r_2}^2)^{-1/2}\frac{Ax_{r_1}x_{r_2}+\cancel{Bx_{r_2}^2}+Cx_{r_2}-B(x_{r_1}^2+\cancel{x_{r_2}^2})}{x_{r_1}^2+x_{r_2}^2+(Ax_{r_1}+Bx_{r_2}+C)^2}\\ &= (x_{r_1}^2+x_{r_2}^2)^{-1/2}\frac{Ax_{r_1}x_{r_2}+Cx_{r_2}-Bx_{r_1}^2}{x_{r_1}^2+x_{r_2}^2+(Ax_{r_1}+Bx_{r_2}+C)^2}\end{aligned}$$

Bibliography

Vincent Aidala and Sherry Hammel. Utilization of modified polar coordinates for bearings-only tracking. *IEEE Transactions on Automatic Control*, 28(3): 283–294, 1983. doi: 10.1109/TAC.1983.1103230.

Yaakov Bar-Shalom and Xiao-Rong Li. *Estimation and Tracking: Principles, Techniques and Software*. Artech House, Inc., 1993.

Sriramya Bhamidipati and Grace Xingxin Gao. Locating multiple GPS jammers using networked UAVs. *IEEE Internet of things journal*, 6(2):1816–1828, 2019.

Jahshan A. Bhatti, Todd E. Humphreys, and Brent M. Ledvina. Development and demonstration of a TDOA-based GNSS interference signal localization system. In *Proceedings of the 2012 IEEE/ION Position, Location and Navigation Symposium*, pages 455–469, 2012. doi: 10.1109/PLANS.2012.6236915.

Denis Constales, Gregory S. Yablonsky, Dagmar R. D'hooge, Joris W. Thybaut, and Guy B. Marin. Chapter 9 - experimental data analysis: Data processing and regression. In Denis Constales, Gregory S. Yablonsky, Dagmar R. D'hooge, Joris W. Thybaut, and Guy B. Marin, editors, *Advanced Data Analysis & Modelling in Chemical Engineering*, pages 285–306. Elsevier, Amsterdam, 2017. ISBN 978-0-444-59485-3.

Syamantak Datta Gupta, Jun Y. Yu, Mahendra Mallick, Mark Coates, and Mark Morelande. Comparison of angle-only filtering algorithms in 3d using EKF, UKF, PF, PFF, and ensemble KF. In *2015 18th International Conference on Information Fusion (Fusion)*, pages 1649–1656, 2015.

Tina Erlandsson. Angle-only target tracking. Master's thesis, Linköping university, 2007.

Aiguo Fei, Li Wang, and Hongming Zhang. An integrated platoon and UAV system for 3D localization in search and rescue. In *IEEE Conference on Computer Communications Workshops*, pages 144–149. IEEE, July 2020. ISBN 978-1-7281-8695-5. doi: 10.1109/INFOCOMWKSHPS50562.2020.9162755.

Eli Fogel and Motti Gavish. Nth-order dynamics target observability from angle measurements. *IEEE Transactions on Aerospace and Electronic Systems*, 24(3): 305–308, 1988. doi: 10.1109/7.192098.

Fredrik Gustafsson. *Adaptive Filtering and Change Detection*. Wiley, 2000.

Fredrik Gustafsson. *Statistical Sensor Fusion*. Studentlitteratur AB, third edition, 2018.

Hsin-Hsiung Huang, Chuhsing Kate Hsiao, and Su-Yun Huang. Nonlinear regression analysis. In *International Encyclopedia of Education (Third Edition)*, pages 339–346. Elsevier, Oxford, third edition edition, 2010. ISBN 978-0-08-044894-7. doi: 10.1016/b978-0-08-044894-7.01352-x.

Inone Joo and Cheonsig Sin. Jammer localization method using degradation of GPS C/No measurements. In *The Fourteenth International Conference on Wireless and Mobile Communications*, number 14, pages 2901–2920. ICWMC, 2018.

Simon J. Julier and Jeffrey K. Uhlmann. A new extension of the Kalman filter to nonlinear systems. In *Proceedings of SPIE 3068: Signal Processing, Sensor Fusion, and Target Recognition VI*, 1997. doi: 10.1117/12.280797.

Simon J. Julier, Jeffrey K. Uhlmann, and Hugh F. Durrant-Whyte. A new approach for filtering nonlinear systems. In *Proceedings of 1995 American Control Conference - ACC'95*, volume 3, pages 1628–1632, 1995. doi: 10.1109/ACC.1995.529783.

Farshad Koohifar, Abhaykumar Kumbhar, and Ismail Guvenc. Receding horizon Multi-UAV cooperative tracking of moving RF source. *IEEE Communications Letters*, 21(6):1433–1436, 2017.

Lantmäteriet. Höjddata, grid 50+. `https://www.lantmateriet.se/sv/Kartor-och-geografisk-information/geodataprodukter/produktlista/hojddata-grid-50`, Last accessed on 2021-03-16.

Ali Mehrjouyan and Alireza Alfi. Robust adaptive unscented kalman filter for bearings-only tracking in three dimensional case. *Applied Ocean Research*, 87: 223–232, 2019.

Gary Miller and Jing Minkler. *Theory and Application of Kalman Filtering*. Magellan Book Company, 1993.

Ryan H. Mitch, Mark L. Psiaki, Brady W. O'Hanlon, Steven P. Powell, and Jahshan A. Bhatti. Civilian GPS jammer signal tracking and geolocation. In *Proceedings of the 25th International Technical Meeting of the Satellite Division of The Institute of Navigation (ION GNSS 2012)*, number 25, pages 2901–2920, September 2012.

Max Nyström. GNSS interference localization through PDOA-Methods. Master's thesis, Luleå University of Technology, 2017.

Marc Oispuu and Marek Schikora. Multiple emitter localization using a realistic airborne array sensor. In *14th International Conference on Information Fusion*, pages 1–8, 2011.

Mikael Olofsson. *Signal Theory*. Studentlitteratur AB, first edition, 2011.

Branko Ristic and M.Sanjeev Arulampalam. Tracking a maneuvering target using angle-only measurements: algorithms and performance. *Signal Processing*, 83 (6):1223–1238, 2003.

Sergei A. Schelkunoff. A mathematical theory of linear arrays. *The Bell System Technical Journal*, 22(1):80–107, 1943. doi: 10.1002/j.1538-7305.1943.tb01306.x.

Ralph Schmidt. Multiple emitter location and signal parameter estimation. *IEEE Transactions on Antennas and Propagation*, 34(3):276–280, 1986. doi: 10.1109/TAP.1986.1143830.

Reza M. Vaghefi, Mohammad Reza Gholami, and Erik G. Ström. Bearing-only target localization with uncertainties in observer position. In *2010 IEEE 21st International Symposium on Personal, Indoor and Mobile Radio Communications Workshops*, pages 238–242, 2010. doi: 10.1109/PIMRCW.2010.5670370.

Eric A. Wan and Rudolph Van Der Merwe. The unscented Kalman filter for nonlinear estimation. In *Proceedings of the IEEE 2000 Adaptive Systems for Signal Processing, Communications, and Control Symposium (Cat. No.00EX373)*, pages 153–158, 2000. doi: 10.1109/ASSPCC.2000.882463.

Zhonghai Wang, Genshe Chen, Erik Blasch, Khanh Pham, and Robert Lynch. Jamming emitter localization with multiple UAVs equipped with smart antennas. In *Proceedings of SPIE - The International Society for Optical Engineering, Automatic Target Recognition XX; Acquisition, Tracking, Pointing, and Laser Systems Technologies XXIV; and Optical Pattern Recognition XXI*, 2010. doi: 10.1117/12.849787.

Wenyuan Xu, Wade Trappe, Yanyong Zhang, and Timothy Wood. The feasibility of launching and detecting jamming attacks in wireless networks. In *Proceedings of the ACM international symposium on mobile ad hoc networking and computing*, number 6, pages 46–57. ACM, May 2005. ISBN 978-1-59593-004-0. doi: 10.1145/1062689.1062697.